Received: 22 July 2020 | Revised: 2 February 2021 | Accepted: 6 February 2021

DOI: 10.1002/jnr.24819

TECHNICAL REPORT

JOURNAL OF Neuroscience Research

Ground state depletion microscopy as a tool for studying microglia–synapse interactions

Patrick Jarmo Paasila[1] | Sandra Y. Y. Fok[2] | Neftali Flores-Rodriguez[3] | Sujata Sajjan[4] | Adam J. Svahn[4] | Claude V. Dennis[1] | R. M. Damian Holsinger[4] | Jillian J. Kril[1] | Thomas S. Becker[4] | Richard B. Banati[4,5] | Greg T. Sutherland[1] | Manuel B. Graeber[4]

[1]Faculty of Medicine and Health, Charles Perkins Centre and School of Medical Sciences, The University of Sydney, Camperdown, NSW, Australia

[2]Biomedical Imaging Facility, Mark Wainwright Analytical Centre, University of New South Wales Sydney, Kensington, NSW, Australia

[3]Charles Perkins Centre, Sydney Microscopy and Microanalysis, The University of Sydney, Camperdown, NSW, Australia

[4]Faculty of Medicine and Health, Brain and Mind Centre, The University of Sydney, Camperdown, NSW, Australia

[5]Life Sciences, Australian Nuclear Science and Technology Organisation, Kirrawee, NSW, Australia

Correspondence
Manuel B. Graeber, Faculty of Medicine and Health, Brain and Mind Centre, The University of Sydney, 94 Mallett St., Camperdown, Sydney, NSW 2050, Australia.
Email manuel.graeber@sydney.edu.au

Funding information
Faculty of Medicine and Health, The University of Sydney; Australian Research Council; National Institute of Alcohol Abuse and Alcoholism

Abstract

Ground state depletion followed by individual molecule return microscopy (GSDIM) has been used in the past to study the nanoscale distribution of protein co-localization in living cells. We now demonstrate the successful application of GSDIM to archival human brain tissue sections including from Alzheimer's disease cases as well as experimental tissue samples from mouse and zebrafish larvae. Presynaptic terminals and microglia and their cell processes were visualized at a resolution beyond diffraction-limited light microscopy, allowing clearer insights into their interactions *in situ*. The procedure described here offers time and cost savings compared to electron microscopy and opens the spectrum of molecular imaging using antibodies and super-resolution microscopy to the analysis of routine formalin-fixed paraffin sections of archival human brain. The investigation of microglia–synapse interactions in dementia will be of special interest in this context.

KEYWORDS

Alzheimer disease, ground state depletion followed by individual molecule return microscopy, microglia, post-mortem archival human brain tissue, super-resolution microscopy, synapses, zebrafish, RRID:AB_141874, RRID:AB_2199013, RRID:AB_2286948, RRID:AB_2534072, RRID:AB_2534076, RRID:AB_2535731, RRID:AB_2536183, RRID:AB_2633277, RRID:AB_324660, RRID:AB_839504, RRID:SCR_013726, RRID:SCR_001622, RRID:SCR_002285, RRID:SCR_002798, RRID:SCR_013673

1 | INTRODUCTION

Advances in microscopy research have facilitated the development of various techniques of super-resolution microscopy which overcome the diffraction limits of light that constrain confocal and two-photon microscopy (Galbraith & Galbraith, 2011). Single molecule localization microscopy (SMLM) techniques perform two basic operations for image reconstruction: (a) the super-localization of single emitters within the nanometer range and (b) the active control of emitters to reduce the concentration of fluorescing molecules at any one time

Patrick Jarmo Paasila and S. Y. Y. Fok contributed equally.

Edited by Christopher Anderson and Junie Warrington. Reviewed by Eamonn Dickson, Bryan Heit, and Mike Jackson.

thus ensuring minimal overlap across a sequence of imaging frames. Single-molecule active control microscopy (SMACM) is a term applied to the various techniques whereby the active control of fluorescent molecules is achieved for the generation of pointillist images (Fölling et al., 2008; Schermelleh et al., 2010; Thompson et al., 2012).

Ground state depletion followed by individual molecule return microscopy (GSDIM) represents one such method of active control and is capable of achieving resolutions down to 20 nm in the lateral dimension (Bretschneider et al., 2007; Hell, 2007; Moerner, 2012). This translates into an approximately 10-fold improvement over the power of resolution of conventional confocal methods. In conventional confocal microscopy, molecules are driven from the ground state into a singlet excited state followed by a dark triplet state that lasts on the order of milliseconds, a period which is too short to ensure a low enough density of active emitters required for SMACM (Thompson et al., 2012). In GSDIM, sufficiently high power is applied to molecules cycling through the standard energy levels in order to drive them into a longer-lived dark state which lasts on the order of seconds, thereby reducing the number of molecules returning to the ground state from which they can be activated once more (hence "ground state depletion") and thus satisfying the conditions required for SMACM. The "blinking" events of single molecules that cycle through energy levels and stochastically return to their ground state with the emission of fluorescent light are recorded over time for image reconstruction (Fölling et al., 2008; Watanabe et al., 2014).

SMACM has been successfully used to study the nanoscale distribution of proteins and their co-localization, revealing molecular interactions that form part of biological processes in eukaryotic cells (Lalkens et al., 2012) and bacteria (Coltharp & Xiao, 2012). However, to date few studies have been performed on multicellular biological samples (Dani et al., 2010; Sigrist & Sabatini, 2012; Vaziri et al., 2008). In this study we present the results of the successful application of GSDIM to tissue from different species: frozen and formalin-fixed paraffin-embedded sections (mouse; human), as well as whole mounts of zebrafish larvae. Our focus is on human brain tissue and specifically the interaction of microglia and synapses in dementia.

Microglia originate from the yolk sac during early embryonic development (Ginhoux et al., 2013), although a small portion, derived from bone marrow precursors, enter the central nervous system (CNS) postnatally (Chen et al., 2010). Microglia in their normal state exhibit a ramified morphology with a territorial coverage of 30%–40% on average in the human cortical parenchyma (Paasila et al., 2019). Microglia are not part of the glial syncytium—they lack gap junctions and thus electrophysiological coupling between individual cells (Eugenín et al., 2001; Wasseff & Scherer, 2014). Microglia are the resident tissue macrophages of the CNS and act as sensors of pathology (Kreutzberg, 1996). However, this is not their most important function because they do not display a macrophage phenotype in healthy normal brain (diseases are exceptional states and not the norm). Maintenance of synaptic integrity appears to be their normal function (Graeber, 2010). Microglia are dynamic cells whose processes are continuously in motion, monitoring their local microenvironment (Nimmerjahn et al., 2005), and intermittently contact neighboring synapses (Nimmerjahn et al., 2005; Schafer et al., 2013; Wake et al., 2009). They respond rapidly to changes in their local environment and may also migrate to sites of tissue injury where they are capable of clearing cellular debris. Thus, microglia have a key role in CNS tissue maintenance and repair as well as in defense mechanisms and notably in inflammatory responses. Importantly, however, microglial activation is not synonymous with neuroinflammation (Svahn et al., 2014). The latter term is highly ambiguous (Graeber, 2014) and thus best avoided, a view also supported by the finding that microglial activation is independent of TSPO, the 18-kDa translocator protein situated on the outer mitochondrial membrane (Banati et al., 2014). In contrast, the normal role of microglia in the development of synaptic connections (synaptic pruning) (Paolicelli et al., 2011) and in the maintenance of synaptic integrity, their apparent normal function (Graeber, 2010) is increasingly appreciated (Ji et al., 2013; Lim et al., 2013; Miyamoto et al., 2013; Parkhurst et al., 2013; Tremblay et al., 2010; Wu et al., 2015; Zhan et al., 2014). Here we have used GSDIM to visualize interactions between microglia and synapses in physiological and pathological conditions.

Significance

We present the use of super-resolution microscopy to detect the internalization of presynaptic material by microglia in the brain of different species *in situ*. Here we demonstrate that the methodology can be applied to routine formalin-fixed paraffin-embedded archival sections of human brain allowing for the study of synapses at high resolution without the need for electron microscopy. Brain tissue from Alzheimer's disease cases and non-demented controls with or without Alzheimer's disease-type pathology are employed to demonstrate this powerful approach. The best studied model of post-traumatic synaptic plasticity, the rodent facial nucleus paradigm, is used for comparison and processes of mouse microglia surrounding axotomized motor neurons are shown to contain focal synaptophysin immunoreactivity. In addition, we illustrate that whole mounts of zebrafish larvae are amenable to the application of this technique. Importantly, we also show enhanced co-localization at a resolution of 20 nm/pixel demonstrating increased intracellular uptake of presynaptic material into microglia cell processes in Alzheimer's disease.

2 | METHODS

2.1 | Sample preparation

2.1.1 | Human tissue sections

Immunofluorescence staining

Following ethics approval from University of Sydney Human Research Ethics Committee (HREC #2019/531), seven micrometer

thick formalin-fixed paraffin-embedded sections of the superior frontal gyrus from four Alzheimer's disease cases (AD), four non-AD control brains, and three non-demented controls with Alzheimer's changes (CAc) that satisfied a Braak stage III or IV were obtained from the NSW Brain Tissue Resource Centre and mounted on glass coverslips (Table 1). One additional non-AD case where the tissue block was exposed to just 24 hr (hrs) fixation (non-AD PC 1) was supplied and is included here as a positive control for comparison to other archival sections examined here with variable fixation periods (Table 1). Blind ID numbers which were written on 6-well plates for free-floating sections were assigned to each section by the experimenter who remained blind to cases and controls until after completing image analysis. Preparation of human brain tissue was performed as previously published (Sutherland et al., 2016). Sections were dewaxed in three, 5-min washes in xylene, and rehydrated by washing for 5 min in 100%, 95%, 70%, and 50% ethanol. Sections underwent heat-induced epitope retrieval in 10 mM Tris/1 mM EDTA (pH 8.5) at 110°C for 30 min in a decloaking chamber (DC2002, BioCare medical, Concord, United States). Aldehyde-related fluorescence was quenched by washing sections twice for 5 min on ice in freshly prepared, effervescent 0.1% sodium borohydride diluted in 0.01 *M* (1×) PBS. Sections were subsequently washed five times for 5 min in 1× PBS containing 0.3% tween-20 (PBST; pH 7.4). Blocking was performed in 10% NGS (Cat# 16210-072, Thermo Fisher Scientific, Waltham, Massachusetts, United States) diluted in 1× PBST followed by primary antibody incubation (anti-ionized calcium-binding adaptor molecule 1 (Iba1), 1:1,000, Cat# 019-19471, FUJIFILM Wako Pure Chemical Corporation, Osaka, Japan, RRID:AB_839504; anti-synaptophysin (Syp), 1:200, Cat# M0776, Dako, Denmark, RRID:AB_2199013), and secondary antibody incubation (1:500; Alexa Fluor (AF) 532 goat anti-rabbit, Cat# A32728, RRID:AB_2534076; Alexa Fluor 647 goat anti-mouse, Cat# A11009, RRID:AB_2633277; ThermoFisher Scientific), both in 1% NGS at 4°C overnight with gentle agitation. Sections were then washed five times for 5 min in 1× PBS. Previously, sections for GSDIM (imaged according to old gold-standard acquisition settings) were stained as described here but incubated in AF 647 (1:200, donkey anti-rabbit, Cat# A-31573, ThermoFisher Scientific, RRID:AB_2536183) and AF 568 (1:200; goat anti-mouse, Cat# A11004, ThermoFisher Scientific, RRID:AB_2534072) and quenched using 0.1% Sudan Black B (BDH Laboratory Chemical Group, United Kingdom) in 70% ethanol for 4 min, then stored in 1× PBS at 4°C until imaging. Further methodological information can be found in the Supporting Information Methods. Table 2 lists all antibodies used here.

2.1.2 | Brain tissue from mice

Mice were held in a secure licensed facility at the Australian Nuclear Science and Technology Organisation (ANSTO, Kirrawee DC NSW 2232, Australia; Licensing body, NSW Department of Primary Industries) in accordance with regulations set out by the Animal Care and Ethics Committee (ACEC). Mice were housed in a temperature-controlled room which was maintained under a 12-hr light/dark cycle. The housing density of mice was 1–5 per cage, depending on behavior. Food and water were made available to the mice ad libitum as well as appropriate bedding and environmental enrichment (Supplier, Gordon's Specialty Stockfeed).

TABLE 1 Basic clinical data of human cases used in this study

Case	Age	Sex	Cause of death	ABC score[a]	Post-mortem Interval (hrs)	Fixation time (wks)	Brain pH
AD 1	83	F	Uremia	A3 B3 C2	3	265	5.9
AD 2	77	M	Aspiration pneumonia	A3 B3 C2	26	52	6.3
AD 3	85	F	Cardiorespiratory failure	A3 B3 C3	10	60	5.9
AD 4[b]	78	F	Cardiac failure	A[d] B3 C[d]	6	3	6.6
Non-AD Control 1[c]	59	M	Pulmonary emboli	A0 B0 C0	29	17	6.6
Non-AD Control 2	69	M	Atherosclerotic cardiac disease	A3 B1 C3	16	421	6.6
Non-AD Control 3	78	F	Pulmonary fibrosis	A0 B0 C0	11	339	6.3
Non-AD Control 4	74	F	Breast and liver cancer with bone metastases	A3 B1 C3	20	83	6.6
CAc 1	85	M	Colorectal cancer and severe cachexia	A2 B2 C3	9	265	6.6
CAc 2	87	F	Metastatic breast cancer	A2 B2 C0	5	148	6.4
CAc 3	102	F	Acute renal failure	A2 B2 C2	5	152	5.9
Non-AD PC 1	94	F	Cardiorespiratory arrest	[d]	43	24 (hr)	[d]

[a]According to the National Institute on Aging-Alzheimer's Association guidelines (Hyman et al., 2012; Montine et al., 2012).

[b]Excluded from the Iba1/Syp co-localization study due to missing data and tissue availability.

[c]Excluded from the Iba1/Syp co-localization study due to tissue availability.

[d]Data unavailable.

TABLE 2 List of antibodies

Name	Immunogen	Origin	Concentration
Anti-Ionized calcium binding adaptor molecule 1 (Iba1)	Synthetic peptide corresponding to the C-terminus of Iba1	Manufacturer: Wako Catalogue: 019-19471 RRID:AB_839504 Host species: Rabbit Target: Human Iba1 Type: Primary, polyclonal	1:1,000
Anti-Synaptophysin (Syp)	A recombinant protein fragment corresponding to the C-terminal cytoplasmic domain of human Syp	Manufacturer: Dako (now Agilent) Catalogue: M0776 RRID:AB_2199013 Host species: Mouse Target: Human Syp Type: Primary, monoclonal (SY38)	1:200
Anti-Syp	Synaptophysin presynaptic vesicles	Manufacturer: AbD Serotec (now Bio-Rad) Catalogue: 8479-0004 RRID:AB_2286948 Host species: Rabbit Target: Mouse Syp Type: Primary, monoclonal (SY38)	1:100
Anti-Cluster of differentiation 11b (Cd11b)	T cell enriched splenocytes from B10 mice	Manufacturer: AbD Serotec (now Bio-Rad) Catalogue: MCA74GA RRID:AB_324660 Host species: Rat Target: Mouse Cd11b Type: Primary, monoclonal (5C6)	1:100
Alexa Fluor 532	Structure: Whole antibody; gamma immunoglobins Heavy and Light chains	Manufacturer: ThermoFisher Scientific Catalogue: A-11009 RRID:AB_2534076 Host species: Goat Target: Anti-rabbit IgG Type: Secondary, polyclonal	1:500
Alexa Fluor 647	Structure: Whole antibody; gamma immunoglobins Heavy and Light chains	Manufacturer: ThermoFisher Scientific Catalogue: A32728 RRID:AB_2633277 Host species: Goat Target: Anti-mouse IgG Type: Secondary, polyclonal	1:500

(Continues)

TABLE 2 (Continued)

Name	Immunogen	Origin	Concentration
Alexa Fluor 568	Structure: Whole antibody; gamma immunoglobins Heavy and Light chains	Manufacturer: Molecular Probes, Invitrogen; now ThermoFisher Scientific Catalogue: A-11077 RRID:AB_141874 Host species: Goat Target: Anti-rat IgG Type: Secondary, polyclonal	1:200
Alexa Fluor 633	Structure: Whole antibody; gamma immunoglobins Heavy and Light chains	Manufacturer: Molecular Probes, Invitrogen; now ThermoFisher Scientific Catalogue: A-21070 RRID:AB_2535731 Host species: Goat Target: Anti-rabbit IgG Type: Secondary, polyclonal	1:200
Alexa Fluor 647	Structure: Whole antibody; gamma immunoglobins Heavy and Light chains	Manufacturer: Molecular Probes, Invitrogen; now ThermoFisher Scientific Catalogue: A-31573 RRID:AB_2536183 Host species: Donkey Target: Anti-rabbit IgG Type: Secondary, polyclonal	1:200
Alexa Fluor 568	Structure: Whole antibody; gamma immunoglobins Heavy and Light chains	Manufacturer: ThermoFisher Scientific Catalogue: A-11004 RRID:AB_2534072 Host species: Goat Target: Anti-mouse IgG Type: Secondary, polyclonal	1:200

Facial nerve axotomy was carried out in accordance with a surgical protocol approved by the University of Sydney Animal Ethics Committee (AEC 2013/5856). In brief, mice were anaesthetized using isoflurane and the right facial nerve transected at its exit from the stylomastoid foramen (for review see [Moran & Graeber, 2004]). After different survival times (Sajjan et al., 2014), the brain stem was removed, embedded in Tissue-Tek® O.C.T compound (Cat# IA018, ProSciTech, Kirwan, Queensland, Australia) and stored at −70°C until further processing. Sixteen micrometer thick coronal sections were cut on a Leica cryostat and collected on coverslips (ProSciTech). Coverslips were immersed in 3.7% methanol-stabilized formaldehyde in 1 × PBS followed by 2-min long incubations in cold acetone (50%, 100%, and 50%). For the reproduction experiment (Graeber et al., 1988) shown in Figure 1, a 1-year-old male mouse was sacrificed 3 days after the operation (Banati et al., 2014). Sections were incubated in a mixture of anti-CD11b (1:100, Cat# MCA74GA, AbD Serotec, Oxford, United Kingdom, RRID:AB_324660) and anti-Syp antibodies (1:100, Cat# 8479-0004, AbD Serotec, RRID:AB_2286948) for 2 hr in a humidified chamber at room temperature. Sections were then rinsed twice in 1× PBS and a secondary antibody mixture (AF 568, Cat# A-11077, RRID:AB_141874; AF 633, Cat# A-11031, RRID:AB_2535731; Molecular Probes, Oregon, United States) was applied for 1 hr at room temperature. Finally, sections were rinsed twice in 1× PBS and stored at 4°C until imaged.

2.1.3 | Whole mounts of zebrafish larvae

Zebrafish larvae were maintained under optimal conditions (Westerfield, 2000) and in accordance with experimental protocols approved by the University of Sydney Animal Ethics Committee (AEC 2013/5591). Adult fish were housed in 4 L tanks maintained at 28.5°C on a 14/10 hr light/dark cycle with twice daily feeding of artemia and protein pellets. Larvae were obtained from natural

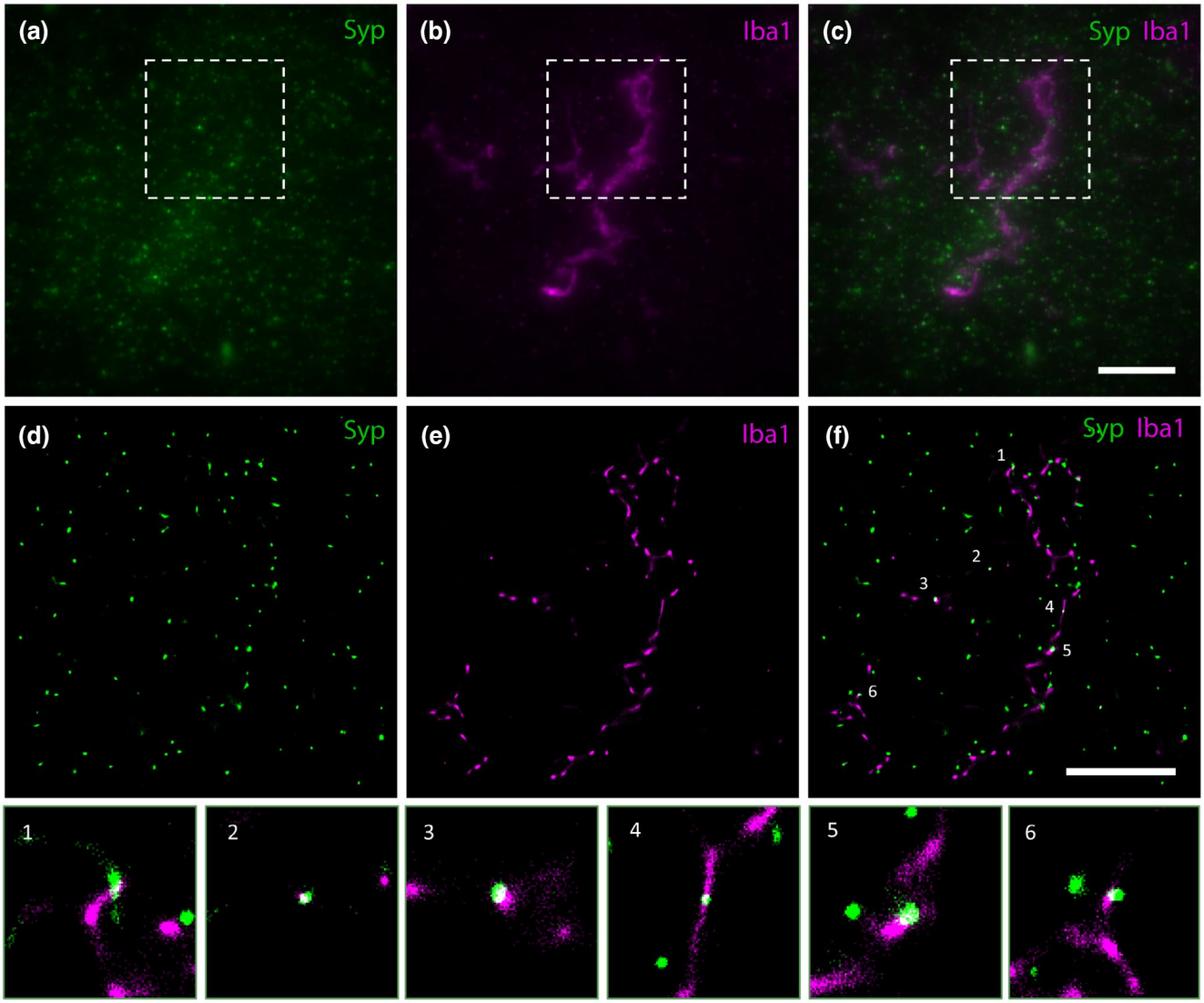

FIGURE 1 (a–c) Widefield epifluorescence images of (a) Syp-immunostaining of presynaptic boutons, (b) Iba1-immunostaining of a microglia profile, and (c) the composite image (case AD 1). Widefield images are shown as maximum intensity projections of 35 z-slices with a depth of 6.65 μm; insets outline the fields of view corresponding to GSDIM reconstructions in the following row (d–f). (d–f) GSDIM reconstruction demonstrating the ability of the technique to display very high resolution images of (d) Syp-immunostaining, (e) Iba1-immunostaining, and (f) the composite image. The numbered spots in (f) highlight overlapping signal (white), that is, Syp-positive presynaptic material inside Iba1-positive microglial cell processes. *Scale bar in c* = 10 μm (a–c), *in f* = 5 μm (d–f) [Color figure can be viewed at wileyonlinelibrary.com]

crossing and eggs were maintained at 28.5°C in E3 medium on a 14/10 hr light/dark cycle. 0.005% 1-Phenyl-2-thiourea (PTU) was added to the E3 medium at 24 hr post-fertilization (pf) to prevent pigmentation. From 5 days pf larvae were fed with paramecia from a culture raised in the facility. Zebrafish sex is indeterminate at embryonic and early larval stages and therefore was not considered as a biological variable here.

For confocal studies, transgenic zebrafish lines expressing mpeg1:mCherry-CAAX were crossed with HCRT:Syp-eGFP resulting in larvae expressing both mpeg1:mCherry-CAAX and HCRT:Syp-eGFP. Larvae expressing both mCherry and eGFP were selected at 3 days pf. For GSDIM studies, transgenic zebrafish expressing mpeg1:eGFP were used 6 days pf. Larvae were euthanized and fixed with 4% paraformaldehyde (pH 7.2) in 1× PBS at room temperature for 2.5 hr and rinsed/stored in 1× PBS at 4°C until use. A total of six larvae were included for GSDIM. Of these, photoswitching was successfully replicated in three.

2.2 | Imaging

2.2.1 | Confocal microscopy

Whole zebrafish larvae were embedded in 1% low melting point agarose. Confocal imaging was performed on a Zeiss LSM 710 confocal microscope using a W Plan-Apochromatic 20×/1.0 NA DIC objective

with 1 airy unit (AU). mCherry was excited with a 568 nm laser line and emission captured on a spectral detector from 570 to 700 nm.

2.2.2 | Ground state depletion followed by individual molecule return microscopy

Mouse and human sections collected onto coverslips were immunolabeled as described above and stored in 1× PBS until imaging. Prior to imaging, sections were first mounted onto "ultracleaned" glass coverslips (Cat# 0107032; 1.5H 18 mm × 18 mm high precision, ±5 μm tolerance; Marienfeld Superior, Lauda-Königshofen, Germany; refer to the Supporting Information Methods for coverslip preparation for GSDIM), and allowed to dry for 10 min before being mounted on depression slides (Cat# 1-6293, neoLab, Heidelberg, Germany) in 100 mM β-mercaptoethylamine (MEA; Sigma, Cat# 30070-10G; dissolved in 36 mM HCl, pH adjusted 8.5; aliquoted and stored at −80°C until imaging), and sealed with silicon glue, Twinsil® (Cat# 13001000, Picodent, Wipperfürth, Germany) or with Bondic® (preferred method; Bondic, Niagara Falls, New York, United States). GSDIM imaging was performed on a Leica SR 3D Ground State Depletion microscope with a Leica HCX PL APO 160×/1.43 NA CORR GSD objective (Leica Microsystems, Wetzlar, Germany). Drift and chromatic aberration are regularly checked on the GSDIM system used here (Sydney Microscopy and Microanalysis, The University of Sydney), and were also checked before and after experiments using 100 nm TetraSpeck™ microspheres (Cat# T7279, ThermoFisher Scientific) imaged using the 488, 532, and 642 nm laser lines. An additional test for drift was also performed using 40 nm FluoSpheres™ (Cat# F8789, ThermoFisher Scientific) and the 642 nm laser line (Supporting Information Methods).

Human brain

Image acquisition parameters were further optimized for imaging human AD archival tissue. For optimal results, the GSDIM system was turned on at least 1 hr before imaging. At least three regions of interest per case, selected at random within the cortical gray matter, were acquired using widefield epifluorescence and GSDIM. Widefield *z*-stacks (up to 7 μm *z*-depth) were acquired using the 160 × GSD objective described above and visualized as maximum intensity projections (*z*-step = 0.19 μm). For GSDIM, an exposure of 11.7 ms, EM gain of 200, and low laser power (2%, 532 nm channel; 4%, 647 nm channel) as for typical super-resolution imaging was used. No pumping or back-pumping was required. Images were acquired over 1 to 3 min, depending on the photo-switching characteristics observed during imaging; with the first 10–30 s being omitted in post-processing using LAS X to eliminate background autofluorescence. A detection threshold of 30 photons/pixel was used for visualization of all GSDIM reconstructions. 3D GSDIM images (0.77 μm *z*-depth) were also acquired using a cylindrical astigmatism lens and following calibration of the Leica GSD system using 80 nm gold beads using the LAS X software wizard. The Z-position of single emitters was determined by taking advantage of the morphology of their astigmatic point spread function by comparing to known morphologies obtained using the gold beads. Internalization of Syp-positive presynaptic material by Iba1-immunolabeled microglia was confirmed by visualizing image reconstructions with orthogonal views for the XZ and YZ dimensions. Negative-primary antibody sections were prepared and viewed concomitantly. Refer to the Supporting Information Methods for further methodological information.

Co-localization study

Here a study was undertaken to investigate the co-localization of Syp- and Iba1-immunolabeling. Eight regions of interest sampled at random between cortical layers III and V from the available three AD cases (AD 1–3 in Table 1), three CAc (CAc 1–3), and three controls (Non-AD Controls 2–4) were acquired from each individual. GSDIM reconstructions were exported as.tif files with a dynamic range set to 0–10 gray values. The 532 and 647 nm channels were then separated and converted to a binary image. Corresponding color channels were then multiplied and filtered to remove "salt and pepper" noise using the "despeckle" algorithm in Fiji in order to find all co-localized positive pixels. Results were displayed as the average percentage of co-localized positive pixels of eight 18 μm^2 regions of interest per case. Image analysis was performed blinded using batch-processing in Fiji (National Institutes of Health, Bethesda, Maryland, United States, RRID:SCR_002285). LAS X was used to export all event lists (in.ascii format) to determine the full width at half maximum (FWHM) of structures of interest, photon counts, localization precision, and for co-cluster analysis.

Mouse and zebrafish

The focus drive on the Leica GSD system is limited to 200 μm. Therefore, in order to prepare whole mounts of zebrafish larvae for GSDIM imaging, a thin layer of head tissue was sliced off with a razor blade under a dissection microscope as the region of interest was slightly deeper than the focus depth of the objective; this also facilitated the diffusion of the MEA buffer into the tissue. The fish larva was then embedded in a drop of 1% low melting point agarose on a depression slide. Once the agarose had set, 100 mM MEA, pH 7.4 was added followed by cover slipping and sealing the sample with Twinsil®. eGFP was excited using a 488 nm laser (excitation bandpass filter 488/10, dichroic longpass mirror 496, and emission bandpass filter 555/100). AF 532 was excited using a 532 laser (excitation bandpass filter 532/10, dichroic longpass mirror 541, and emission bandpass filter 600/100). AF Fluor 647 was excited using a 642 nm laser (excitation bandpass filter 642/10, dichroic longpass mirror 649, and emission bandpass filter 710/100). For GSDIM acquisition, the respective area of interest was "pumped" in epifluorescence mode until molecules began blinking. Acquisition of photons representing molecules returning from the long-lived dark state was carried out in epifluorescence mode and reconstruction of the final GSDIM image was completed

using the Leica Application Suite X (LAS X; Leica Microsystems, RRID:SCR_013673).

2.3 | Statistics

For the aforementioned co-localization study, three AD cases, three CAc, and three controls were included as per tissue availability. Blinding was established by assigning each individual with a random alphanumeric identifier. Blinding was maintained until after statistical analyses had been completed. For the co-localization study, the data were expressed as the mean percentage (of eight regions of interest) of co-localized pixels per standard 18 μm^2 (900 $pixels^2$) field of view per individual. Quantile–quantile (Q–Q) plots of each group were visualized and the normality was tested using the Shapiro–Wilk test. Equality of variances was tested using the Brown–Forsythe test. Group differences were tested by Welch's analysis of variance (ANOVA) (W) with Dunnett's T3 test for multiple comparisons. The mean and standard deviation (*SD*) were determined for each group and a post hoc power analysis to determine effect size (f) was performed using G*Power (*F* test, post hoc ANOVA: fixed effects, omnibus, one-way; RRID:SCR_013726). Groups were controlled for age, sex (which was not disaggregated due to the small group sizes), fixation time, post-mortem index, and brain pH. Spearman ρ was calculated to identify potential correlations between the percentage of co-localized Iba1/Syp pixels and the aforementioned factors. A p value < 0.05 was considered statistically significant. Statistical analyses and scatterplots were performed in GraphPad Prism (GraphPad Software; San Diego, California, United States, RRID:SCR_002798). Event lists (exported from LAS X as.ascii files) were handled using MATLAB (MathWorks, Natick, Massachusetts, United States, RRID:SCR_001622), which was also used to produce the line graphs of photon counts. Table 3 lists all software tools used here.

3 | RESULTS

3.1 | GSDIM as a tool to study the localization of synapses in archival sections of human cerebral cortex

Widefield epifluorescence images (Figure 1a–c) are presented alongside their respective super-resolved pointillist reconstructions (Figure 1d–f), demonstrating the suitability of GSDIM as a tool for studying synapses at high resolution. FWHM of a representative structure of interest in widefield and GSDIM micrographs demonstrates the ability of the GSDIM system used here to achieve super-resolved images (Figure 2a–c). GSDIM reconstructions had a horizontal resolution of 20 nm/pixel and an axial resolution of 50 nm/pixel. Internalization of Syp-immunoreactive presynaptic material by Iba1-positive microglia was demonstrated in AD cortical samples using 3D GSDIM (Figure 3) (Supporting Information Movie 1 and 2 show the 3D GSDIM projection and the corresponding widefield fluorescence image, respectively, of this region of interest). Images showing spurious co-localization in widefield and more certain co-localization in a GSDIM reconstruction of cortical tissue from a control case have also been provided for comparison (Figure 4). Additional images, including a positive-control section from tissue fixed for 24 hr (sample, Non-AD PC 1, Table 1) and TetraSpeck™ microsphere controls are provided in the Supporting Information (Figures S1–S4).

TABLE 3 List of software tools

Software	RRID
MATLAB	RRID: SCR_001622
Fiji	RRID: SCR_002285
G*Power	RRID: SCR_013726
GraphPad Prism	RRID: SCR_002798
Leica Application Suite X	RRID: SCR_013673

3.2 | Study of Iba1/Syp co-localization

Previously we have shown morphological changes in cortical microglia in AD and CAc post-mortem brain tissue (Paasila et al., 2019, 2020). Here it was of interest to investigate the potential of microglia to internalize pre-synaptic material in AD and CAc cases. AD cases ($n = 3$, mean percentage of co-localized pixels = 0.04% ± 0.006 *SD*) showed a higher level of Iba1/Syp signal co-localization compared to CAc ($n = 3$, mean = 0.006 ± 0.0008 *SD*, $p = 0.02$) and controls ($n = 3$, mean = 0.006 ± 0.005, $p = 0.006$; Welch's ANOVA: $n = 9$, W (2.0, 2.8) = 36.1, $p = 0.01$; effect size (f) = 0.8) (Figure 5). Groups did not differ by the percentage of area stained for Iba1 ($n = 9$, W (2.0, 2.8) = 8.2, $p = 0.1$) or Syp ($n = 9$, W (2.0, 3.4) = 4.5, $p = 0.1$). Plots of the number of localizations and photons for both the 532 and 647 nm channels in AD cases, CAc, controls, and background fluorescence can be found in Figure 6a,b. The summary statistics are also presented in Table 4. The frame correlation rate during image acquisition was between 0.25 and 0.5. Exclusion of the first 10–30 s of imaging for GSDIM reconstructions significantly reduced the level of background fluorescence. To further test the quality of reconstructions, a filtration step to exclude all localizations in 10 or more and 2 or more consecutive frames was applied. This resulted in a loss of ~11.1% and ~17.6% of localizations compared to the original reconstruction (which was generated without filtration of localizations occurring in consecutive frames), respectively. Importantly, the overall effect this had on the test reconstructions was minimal compared to the original reconstruction (Figure 7a–e).

The impact of blood vessel in co-localization analyses was negligible as they were not present in the 647 nm channel reconstructions (Figure S5; see also Figure 7 and Figure S4). Autofluorescence due to lipofuscin deposits displayed variable photoswitching characteristics depending on its signal intensity, with only low intensity deposits impacting reconstructions of both channels. Therefore, all

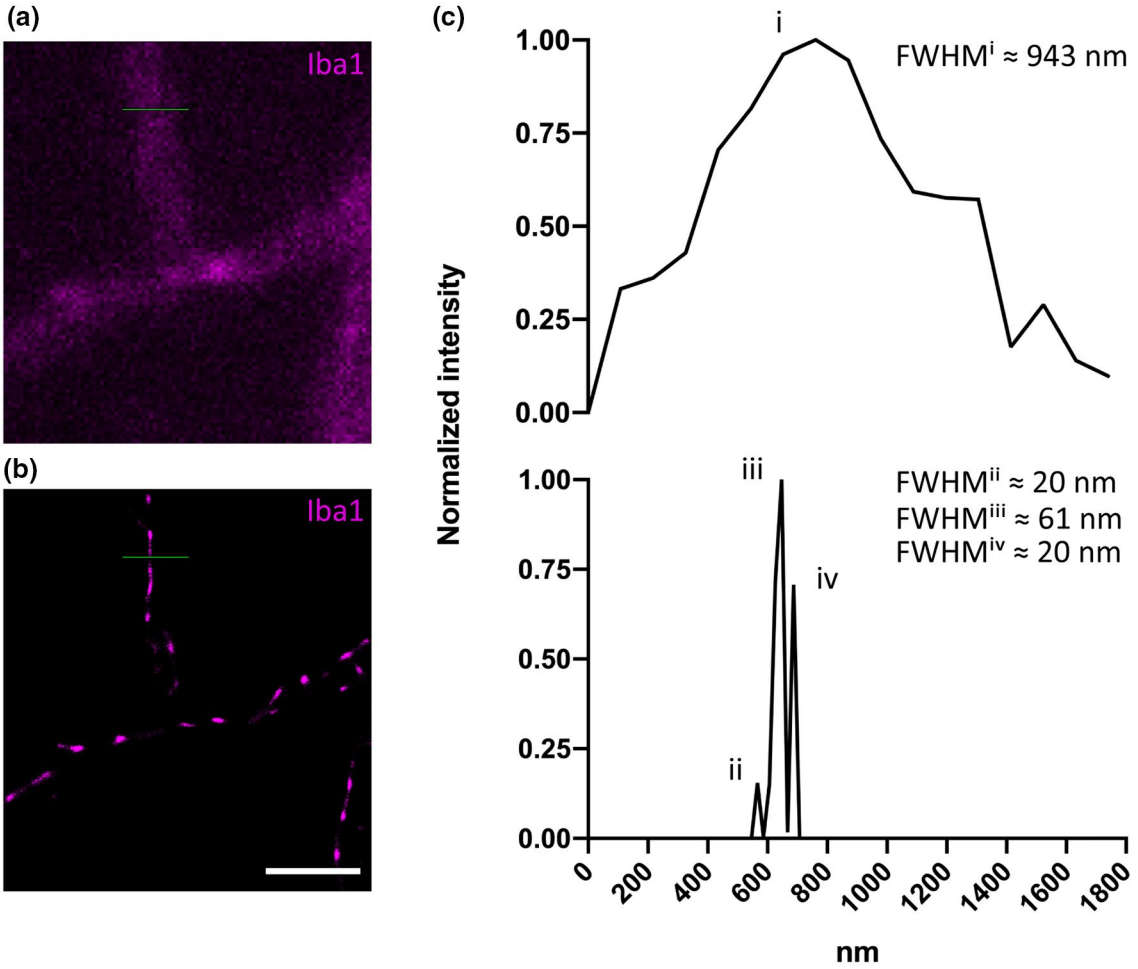

FIGURE 2 (a–b) A representative Iba1-positive (magenta) microglial cell with a typical perpendicularly branching cell process imaged in (a) widefield and (b) GSDIM mode, respectively. (c) Normalized pixel intensity values are plotted against the diameter of the cell process measured in nanometers as marked by the corresponding green line of interest in (a) and (b), respectively. Full width at half maximum (FWHM) of the single peak in the upper chart (marked "i") corresponds to ~943 nm for the widefield image. FWHM of the first ("ii"), second ("iii"), and third ("iv") peak corresponding to the GSDIM reconstruction in (b) is ~20, 61, and 20 nm, respectively. *Scale bar* = 2.5 μm (a,b) [Color figure can be viewed at wileyonlinelibrary.com]

regions of interest imaged here were selected to exclude the presence of lipofuscin. Sudan Black B staining to block lipofuscin autofluorescence was not included here as it was found to significantly impair photoswitching of fluorophores which resulted in non-cycling noise during imaging and greater "smearing" in GSDIM reconstructions (Figure S6).

3.3 | Post-traumatic synaptic stripping in the rodent facial nucleus at super-resolution

GSDIM is less time consuming than conventional transmission electron microscopy (EM). Here GSDIM was employed to examine the mouse facial nucleus 3 days following axotomy to determine whether the technique is suitable for visualizing the involvement of microglial cells in synaptic stripping (Blinzinger & Kreutzberg, 1968). GSDIM revealed occasional microglia containing presynaptic material predominantly within their perineuronal cell processes (Figure 8, insets). The frequency of this observation was in keeping with published EM results indicating that uptake of presynaptic material by microglial cells during synaptic stripping is not a readily discernible phenomenon.

3.4 | Whole mounts of zebrafish larvae are amenable to GSDIM

We further tested whether it was possible to perform GSDIM on whole mounts of transgenic zebrafish larvae. A zebrafish larva expressing mpeg1:eGFP in microglia was subjected to high laser power to induce the long-lived triple dark state and emitter blinking in MEA buffer. We observed that longer pumping times at lower laser intensity were more effective; it took on average 20 min for eGFP to start blinking. Figure 9a represents a GSDIM image reconstruction of a tectal microglia cell. The inset seen in Figure 9a shows an mpeg1-expressing microglial cell at confocal

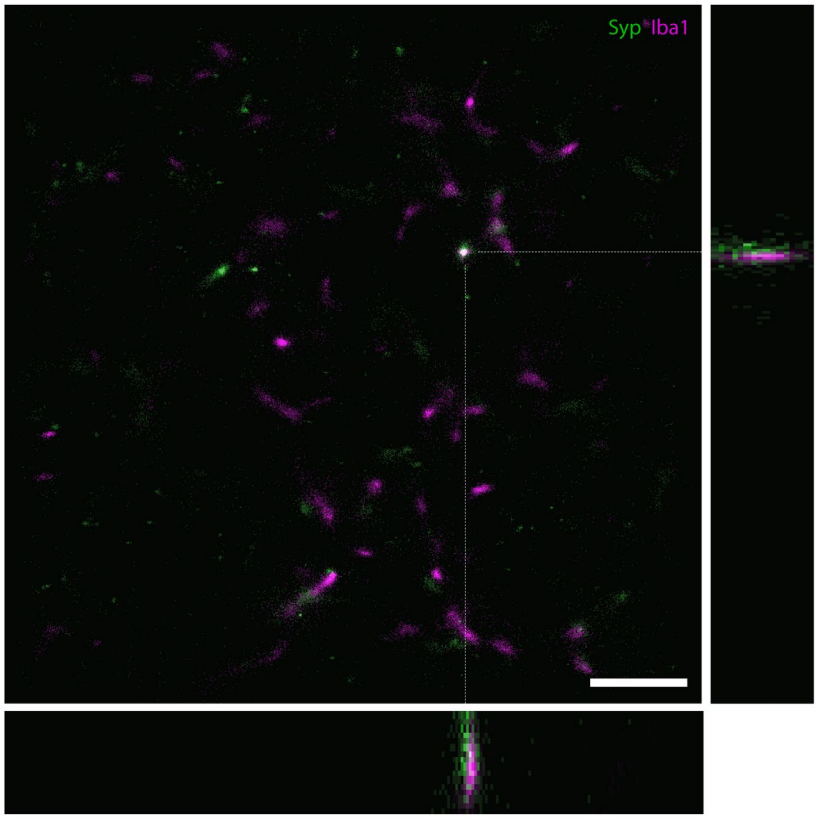

FIGURE 3 A 3D GSDIM reconstruction of part of a microglial cell from case AD 2 with a *z*-depth of 0.77 μm shown as a maximum intensity projection, with orthogonal views of the XZ and YZ dimensions on the bottom and left of the image, respectively. The orthogonal views have been magnified by 1.99× and cropped for better visualization (each view represents a space that is 0.77 μm in the Z-direction × 5.17 μm in the X- and Y-direction, respectively). *Scale bar* = 2.5 μm (XY image only) [Color figure can be viewed at wileyonlinelibrary.com]

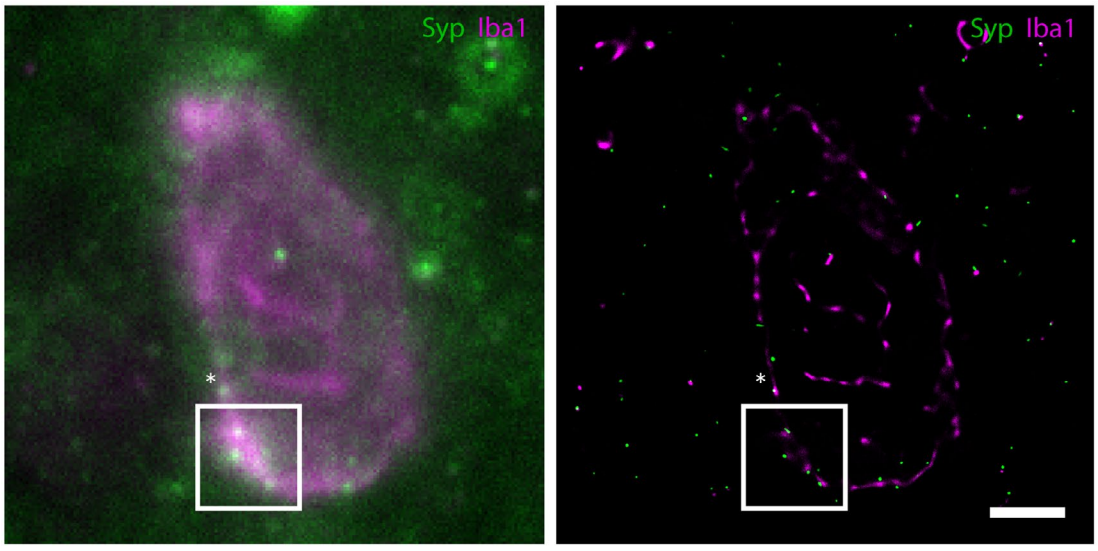

FIGURE 4 A widefield (left) and corresponding GSDIM reconstruction (right) demonstrating Iba1- (magenta) and Syp- (green) immunoreactivity in the dorsolateral prefrontal cortex of control human brain tissue (Non-AD Control 2). The areas marked by the asterisk (*) and within the white box in the widefield image indicate instances of potential co-localization of signals (white, merge color). The GSDIM reconstruction of the corresponding area (white box, right) better able resolves the Iba1- and Syp-positive signals, illustrating the need for GSDIM resolution. The area marked by the asterisk (*) in the GSDIM reconstruction represents an instance of true signal overlap (Syp inside a microglial process; white, merge color). Examples of overlap regions (white) in the GSDIM reconstruction are indicative of Iba1 and Syp molecules that are closer than 20 nm. Scale bar = 2.5 μm [Color figure can be viewed at wileyonlinelibrary.com]

resolution for comparison. Figure 9b–e illustrates selected areas at higher magnification of images captured with GSDIM compared to widefield fluorescence.

4 | DISCUSSION

The technical ability to visualize the spatial relationships of multiple proteins in tissues at super-resolution represents a major capability in the field of microscopy. Applications for studying biological structure with super-resolution microscopy have grown considerably in the last few years (Birk, 2019; Fang et al., 2018; Garcia et al., 2017; Mockl et al., 2014; Schermelleh et al., 2019; Sieben et al., 2018; Sreedharan et al., 2017; Stracy & Kapanidis, 2017; Xu & Liu, 2019) and new advances in the field are predicted to improve our understanding as the potential of the technology is further realized. In the past, studies of microglia in brain tissue were typically conducted using immunocytochemistry in combination with brightfield, epifluorescence widefield, or confocal microscopy (Sarmiento, 2013). However, if more detailed information on cell–cell interactions was required, such as the precise spatial relationships between microglial processes and synaptic boutons, then tissue samples had to be processed for EM. With the invention of super-resolution microscopy, the diffraction limit imposed by conventional light microscopy no longer applies and biological structures can be viewed at a resolution closer to that offered by EM with essentially the same effort that is required for conventional confocal microscopy. Here we have demonstrated the use of GSDIM to show increased co-localization of Iba1-positive microglia and Syp-positive presynaptic material in AD compared to CAc and normal controls.

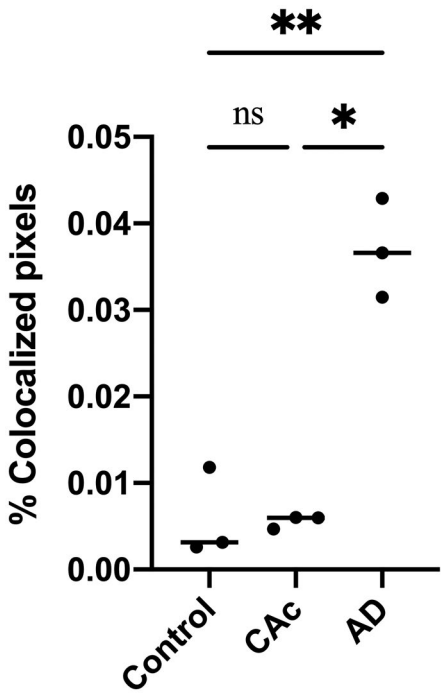

FIGURE 5 Scatterplot demonstrating an elevated average percentage of co-localized pixels per 18 μm^2 (900 $pixels^2$) standard region of interest in AD compared to CAc and controls. $^*p < 0.05$; $^{**}p < 0.01$; ns (not significant), $p > 0.99$

4.1 | Super-resolution imaging of formalin-fixed paraffin-embedded sections of human cerebral cortex

EM is the traditional method for obtaining ultrastructural information on brain tissue, but samples have to be perfusion-fixed ideally and dissected into small pieces measuring only 1–2 mm^3. As a result, images may not be representative due to their small size, necessitating additional experiments. Post-fixation, embedding into plastic, ultrathin sectioning, and contrasting are all labor intensive, costly, and time consuming. Furthermore, while mouse and zebrafish tissue can be easily procured and processed for EM, fresh human tissue samples are much

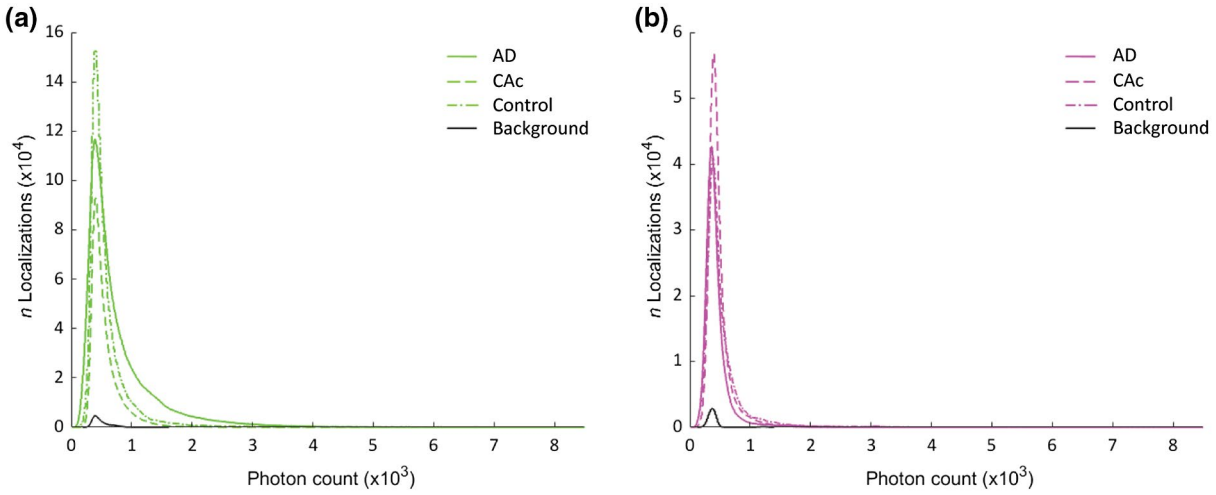

FIGURE 6 (a,b) Plots showing the number of localizations by photon count in both the (a) 647 nm (green) and (b) 532 nm (magenta) channels from Alzheimer's disease (AD) cases, Controls with Alzheimer's changes (CAc), normal controls, and background. Table 2 shows the summary statistics [Color figure can be viewed at wileyonlinelibrary.com]

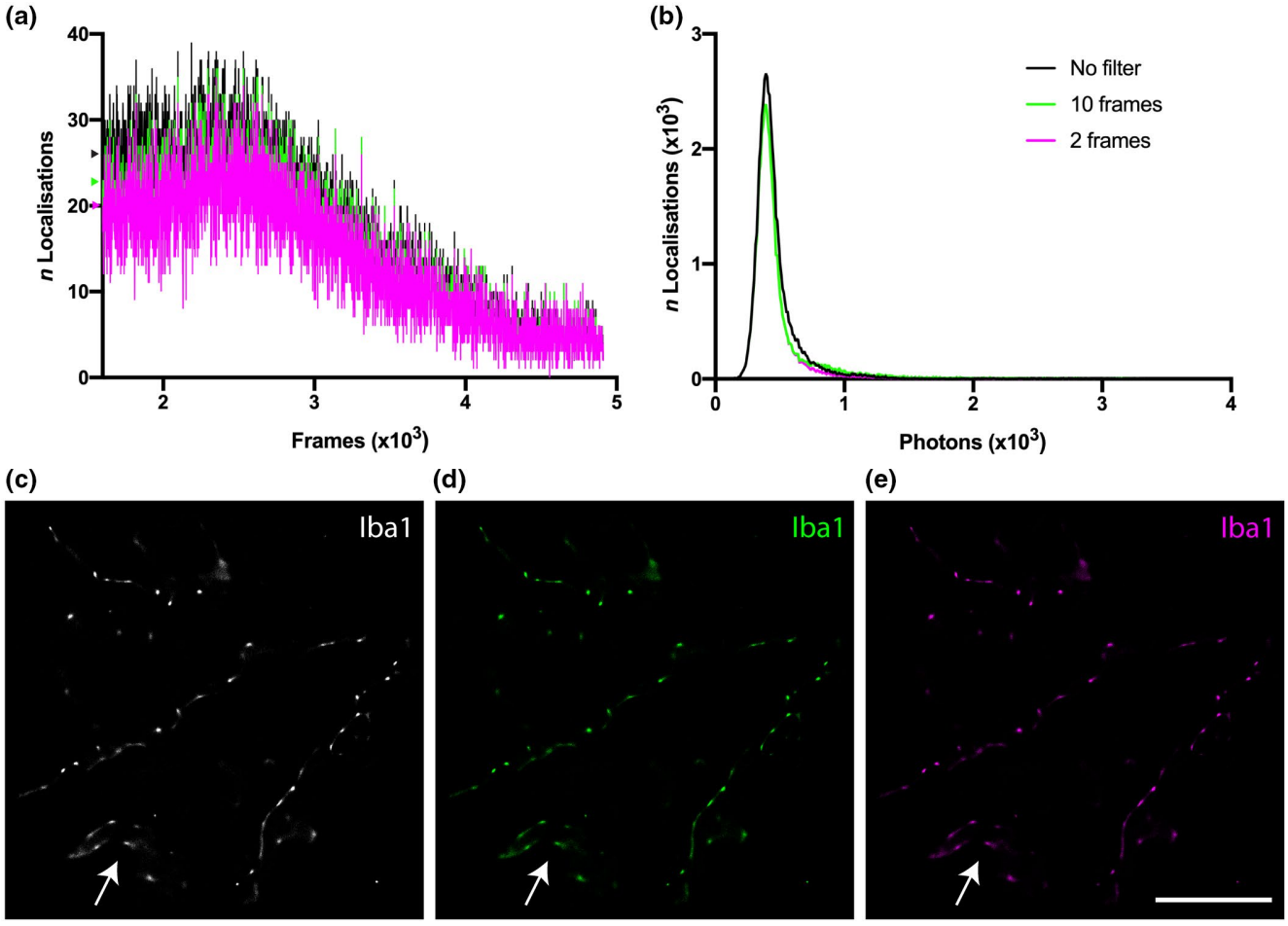

FIGURE 7 A test of the quality of GSDIM reconstructions from unfiltered data was performed in order to determine the impact of localizations that occurred through consecutive imaging frames. (a) "Blinking" events over several thousand frames in unfiltered data (black) and filtered data excluding localizations that occurred in 10 or more (green) and 2 or more (magenta) consecutive frames (the colored markers on the y axis show the shift in the average number of localizations in the first 2×10^3 frames for each filter group). (b) The total number of localizations in the unfiltered data set was 55,006 (black), 48,913 after removing localizations occurring in 10 or more consecutive frames (green), and 45,347 after removing localizations in 2 or more consecutive frames (magenta). c–e GSDIM reconstructions of the respective event lists for (c) unfiltered data (white), and thresholds at (d) 10 (green) and (e) 2 (magenta) consecutive frames were not substantially different (arrow heads indicate Iba1-positive staining in a likely blood vessel—shown in each image). *Scale bar* = 5 μm (c–e) [Color figure can be viewed at wileyonlinelibrary.com]

harder to obtain. However, archives of human brain tissue exist worldwide in neuropathology departments and brain banks in the form of collections of brain tissue retained in fixative and paraffin blocks left over from routine diagnostic procedures. This is of relevance as extended storage in aldehyde fixatives reduces the suitability of CNS tissue for EM (Liu & Schumann, 2014). Therefore, being able to perform GSDIM on routine human paraffin sections opens up new avenues for research. In particular, the approach described in this paper enables the spectrum of molecular imaging methods using antibodies and super-resolution microscopy to be used for high-throughput analyses of common brain diseases and at cheaper cost compared to EM even if tissue has been stored for several years.

Microglia–synaptic interactions in physiological and diseased states are increasingly appreciated. A preprint of one study using confocal microscopy demonstrated increased co-localization of the endosomal/lysosomal marker CD68, expressed by myeloid cells including microglia, and the presynaptic marker synapsin-I in post-mortem human tissue (Tzioras et al., 2019). Here we have used GSDIM to demonstrate increased co-localization of presynaptic material by microglia in post-mortem human AD tissue compared to healthy controls and other non-demented controls with high levels of AD-type pathology. It has long been known that neuronal loss exceeds the burden of neurofibrillary tangles in AD (Gomez-Isla et al., 1997), that microglia neuronal toxicity can be elicited in cell culture (Giulian et al., 1996), and that the loss of synapses best correlates with the severity of dementia (Terry et al., 1991), but there remains a paucity of evidence linking these observations in human studies. Here we show the direct involvement of microglia in synaptic loss in AD. Discontinuities in the Iba1-positive cellular processes, particularly in AD cases seen here (termed "pseudo-fragmentation"), has been previously noted (Paasila et al., 2019, 2020;

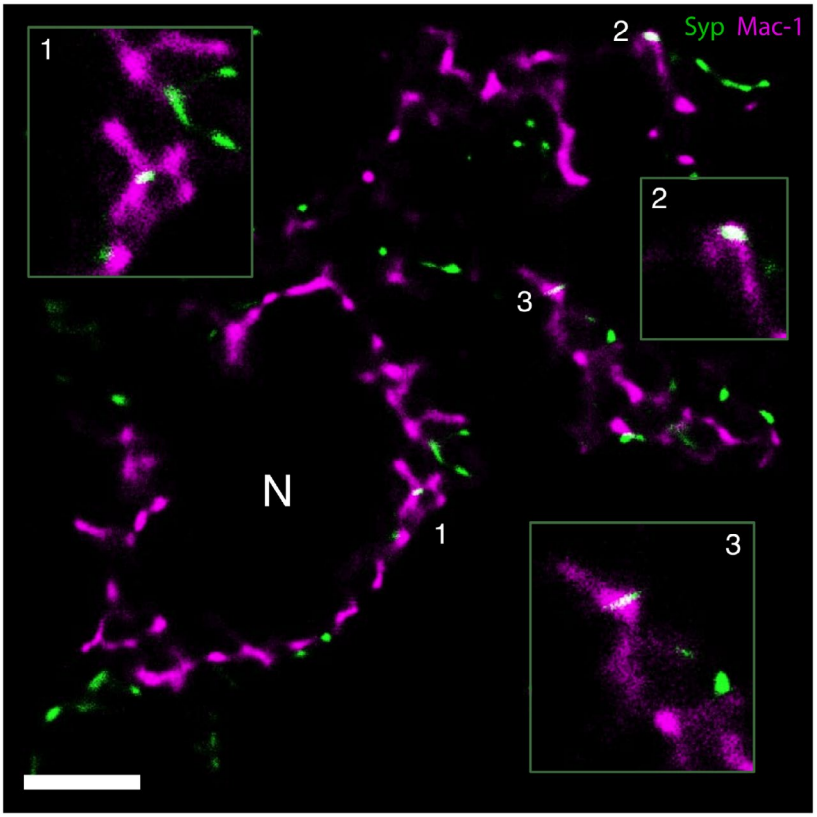

FIGURE 8 GSDIM demonstrates Syp-immunoreactive presynaptic material (green) inside perineuronal microglial processes (Mac-1, magenta) in the axotomized mouse facial nucleus 3 days following axotomy. Examples of stripped synapses (white, merge color) are magnified in the insets. Numbered regions represent the magnified areas in the insets. N marks a cross-sectioned motor neuron. *Scale bar* = 2.5 μm [Color figure can be viewed at wileyonlinelibrary.com]

TABLE 4 Photon counts and total number of localizations

	AD (AF 532)	AD (AF 647)	CAc (AF 532)	CAc (AF 647)	Control (AF 532)	Control (AF 647)	Background (AF 532)	Background (AF 647)
Mean (*n* photons)	432.6940	777.1586	500.1218	566.3529	531.1901	635.8538	394.1738	491.7849
Median (*n* photons)	388.1000	569.5000	428.5000	480.2000	433.0000	478.3000	372.2000	449.6000
Minimum (*n* photons)	13.8000	18.5000	53.2000	58.9000	23.9000	32.9000	136.5000	190.7000
Maximum (*n* photons)	5,222.6000	8,065.3000	12,822.0000	15,146.6000	16,630.6000	14,520.4000	1,393.0000	1,610.9000
SD (*n* photons)	218.6298	616.6569	341.7096	332.1231	393.3020	675.1907	156.7882	153.1452
SEM	0.1465	0.2407	0.2856	0.1998	0.3478	0.4360	1.0304	0.4703
n localizations	2,226,894	6,562,200	1,431,497	2,762,082	1,278,972	2,398,669	23,153	106,033
n ROIs	24	24	24	24	24	24	5	5

Abbreviations: *n*, number of; ROIs, regions of interest; *SEM*, standard error of the mean.

Streit et al., 2009). In fact, such processes remain intact when visualizing cells with an additional marker as has been demonstrated in an EM investigation performed elsewhere (Tischer et al., 2016). Given a recent two-photon imaging study in mice showed that microglia work in concert with astrocytes to phagocytose neuronal apoptotic debris (Damisah et al., 2020) it will also be interesting to see in a larger cohort of AD cases if a similar cooperative underpins physiological synaptic pruning and how this might also interact with a human life-span synaptome architecture (LSA) as described in mouse (Cizeron et al., 2020).

Co-localization studies are commonly employed in biology in order to study spatial relationships between structures or molecules of interest. In broad terms, co-localization of signals can

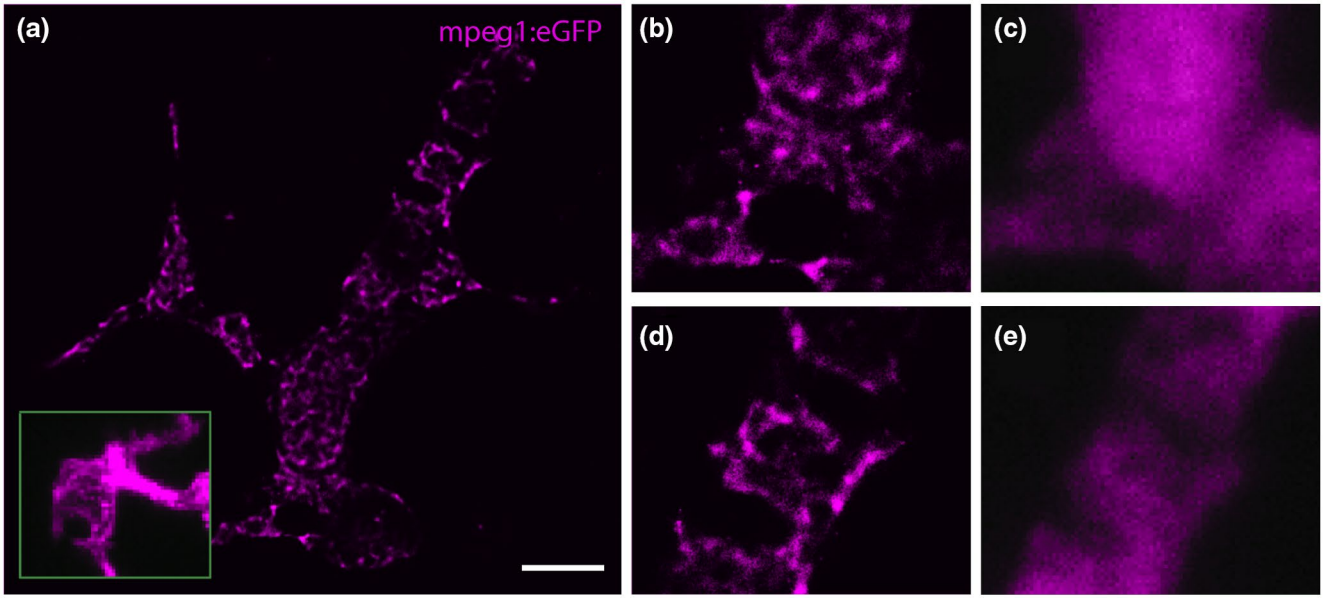

FIGURE 9 (a) GSDIM reveals the intracellular distribution of mpeg1:eGFP (magenta) in microglia in the optic tectum of a zebrafish larva. Inset in a shows an mpeg1:eGFP expressing microglial cell captured with confocal microscopy for comparison. (b,d) Magnified areas from a showing the intracellular distribution of eGFP with their widefield fluorescence images in (c) and (e), respectively. *Scale bar* = 5 μm (a) [Color figure can be viewed at wileyonlinelibrary.com]

be investigated by pixel-based or object-based methods (Bolte & Cordelières, 2006). Pixel-based methods rely on finding correlations between signal intensities whereas object-based methods first segment images and then apply an overlap procedure. Here a simple object-based strategy was pursued to quantify the relative occurrence of Iba1/Syp co-localization (at a resolution of 20 nm/pixel) in AD, CAc, and normal aged brain. However, it is important to note that other advanced spatial interaction analyses for investigating co-localization also exist. Such strategies robustly account for accidental overlap, post-processing errors, and offer additional statistics-based inferences about spatial relationships between objects of interest (Helmuth et al., 2010). Software packages for these types of cluster analyses, such as Mosaic segmentation and Dual parameter Optimization in Histograms (QuASIMoDOH) (Paparelli et al., 2016) and MosaicIA (Shivanandan et al., 2013), are freely available for use in image analysis software such as Fiji, but were outside the scope of this investigation. A recent review also covers many other plugins for processing and analyzing image data acquired from various imaging modalities for use in Fiji (Linde, 2019).

4.2 | GSDIM enables studies of pathological synaptic turnover

Peripheral axotomy of the rodent facial nerve leads to well-characterized changes in its central nucleus of origin. The extrinsic facial motor neurons respond to the loss of their distal axon by activating a cellular regeneration program (Moran & Graeber, 2004). Surrounding facial nucleus glial cells also become involved. Microglia respond by expressing the CR3 complement receptor within hours of the axotomy (Graeber et al., 1988) and undergo mitotic cell division (Yamamoto et al., 2010) after a few days. Astrocytes upregulate their expression of the glial fibrillary acidic protein (GFAP) and reshape their cell processes. Accompanying the axonal reaction, microglial cells engage in a process known as "synaptic stripping" (Blinzinger & Kreutzberg, 1968; Graeber, 2010). This process has two components, an initial detachment of afferent axonal endings from the neuronal somatic membrane and dendrites, followed by the displacement of the detached terminals by microglial cells. It is the latter process followed by astroglial insulation of neurons (Graeber & Kreutzberg, 1988) that appears to be responsible for the long-lasting functional deficit observed in patients with Bell's palsy (Graeber et al., 1993). In functional terms, a facial nerve transection results in what equates to a structural and functional split of the face from the brain. Importantly, the fate of the large number of "stripped" axon terminals is not known in detail. Typical phagocytic macrophages are absent during the entire regeneration period although synaptic boutons have been seen being displaced and even engulfed by microglial processes at the EM level. However, systematic EM studies are costly and very time consuming and therefore specific EM studies to elucidate the fate of the stripped axon terminals have so far not been performed. It is assumed that retraction of afferent neurites plays a major role in the disappearance of free-lying axon boutons during post-traumatic synaptic plasticity in the axotomized rodent facial nucleus. This view is supported by the results of the present study, as the rather limited uptake of synaptic material by microglia in GSDIM is incompatible with large-scale phagocytosis.

A number of studies implicate microglia in synaptic remodeling, internalization, and plasticity in healthy and pathological conditions (Graeber, 2010; Hong et al., 2016; Ji et al., 2013; Lim et al., 2013;

Miyamoto et al., 2013; Paolicelli et al., 2011; Parkhurst et al., 2013; Schafer et al., 2012; Svahn et al., 2014; Tremblay et al., 2010; Tzioras et al., 2019; Vasek et al., 2016; Wake et al., 2009; Wang et al., 2020; Weinhard et al., 2018; Zhan et al., 2014). The majority of studies monitoring microglial interactions with synapses have been conducted using confocal and two-photon microscopy. The advantages of using confocal and two-photon microscopy are that the cellular components in microglia can also be directly labeled and observed, and microglial interactions can even be studied *in vivo*. However, resolution of these microscopic techniques is limited by the diffraction limit of light (Schermelleh et al., 2010). To further elucidate their physiological roles, EM studies of microglia combined with serial sectioning had to be employed, providing new insights into the interaction of microglia and excitatory synapses. For instance, it was discovered that microglia are involved in synaptic plasticity following mere alterations in sensory experience (Tremblay et al., 2010).

4.3 | Super-resolution imaging of transgenic zebrafish larvae

Super-resolution microscopy may be utilized for cultured cells or tissue sections ranging from nanometers to micrometers in thickness by direct or indirect labeling with fluorescent dyes. Fluorophore selection will depend on compatibility with the embedding media used. As demonstrated in this paper, active control of fluorescent probes labeling tissue sections that are several micrometers in thickness can be successfully performed (Galbraith & Galbraith, 2011). Here we demonstrate that molecules expressed *in situ* in whole mount preparations of transgenic zebrafish larvae can be imaged as well. However, it is worth noting that fluorophores linked to antibodies are clearly preferred for the visualization of expressed gene products because endogenously expressed fluorescent proteins yield a much lower intensity in GSDIM (Ries et al., 2012).

In this example, eGFP expressed in microglia was used as the *in situ* expression of fluorophores as it is suitably bright and photostable (Fernandez-Suarez & Ting, 2008). GFP is known for its "blinking properties" (Dickson et al., 1997) and a sizeable population of expressing microglia are consistently present in the tectal region (Svahn et al., 2013). Having an easy to define and comparatively bright cell population minimizes the influence of background fluorescence and out of focus light from neighboring tissue areas which allows for the relatively straightforward reconstruction of super-resolved mpeg1:eGFP microglia. Importantly, this study along with others demonstrates that eGFP, a widely used fluorescent marker, can also be used in super-resolution microscopy (Rankin et al., 2011).

5 | CONCLUSIONS

In this study, we have demonstrated that GSDIM can be used to investigate microglia–synapse interactions in conventional, readily prepared cryostat sections of mouse brain, in whole mount transgenic zebrafish larvae and, most importantly, in 7 μm post-mortem formalin-fixed paraffin-embedded human brain tissue. We have also shown that the uptake of synaptic material is elevated in AD. Continued use of GSDIM will benefit from addressing certain limitations encountered here: reducing background fluorescence, for example, by using thinner tissue sections or by the deactivation of out-of-focus fluorophores as has been demonstrated elsewhere (Dani et al., 2010); by taking greater advantage of the total internal reflection fluorescence (TIRF) capability of the system used here to limit the focal depth of the lasers; by fitting the microscope with a motorized stage and expanding the available software features to include a tilescan and quick spiral functionalities to enable larger previews and automated sampling methodologies as the manual stage operation of the system used here would make it difficult to undertake a larger sampling regime; and increasing sample size with additional consideration for the impact of biological variables such as sex. Lastly, the methods presented here allowed for imaging of human brain samples even with extended storage and the unequivocal identification of Syp/Iba1 co-localized puncta as evidence of contact between synapses and microglia processes.

DECLARATION OF TRANSPARENCY

The authors, reviewers and editors affirm that in accordance to the policies set by the *Journal of Neuroscience Research*, this manuscript presents an accurate and transparent account of the study being reported and that all critical details describing the methods and results are present.

ACKNOWLEDGMENTS

GSDIM was performed at Sydney Microscopy and Microanalysis, Charles Perkins Centre, The University of Sydney. Human tissues were received from the New South Wales Brain Tissue Resource Centre at the University of Sydney which is supported by the National Institute of Alcohol Abuse and Alcoholism (NIH (NIAAA) AA012725). Parts of this work were supported by the Australian Research Council (ARC) grant, DP150104472. GTS is a University of Sydney SOAR Fellow.

CONFLICT OF INTEREST

The authors declare no conflict of interest.

AUTHOR CONTRIBUTIONS

PJP and SYYF performed research, analyzed data, and wrote the paper. PJP designed the co-localization study. SS, AJS, CVD, NFR, RMDH, JJK, TSB, RBB, and GTS performed research and analyzed data. MBG designed the study, performed research, analyzed data, and wrote the paper. All authors contributed to editing the manuscript.

PEER REVIEW

The peer review history for this article is available at https://publons.com/publon/10.1002/jnr.24819.

DATA AVAILABILITY STATEMENT

The data and code for raw data processing and statistical analysis that support the findings of this study are available from the corresponding author upon reasonable request.

REFERENCES

Banati, R. B., Middleton, R. J., Chan, R., Hatty, C. R., Kam, W. W., Quin, C., Graeber, M. B., Parmar, A., Zahra, D., Callaghan, P., Fok, S., Howell, N. R., Gregoire, M., Szabo, A., Pham, T., Davis, E., & Liu, G.-J.. (2014). Positron emission tomography and functional characterization of a complete PBR/TSPO knockout. *Nature Communications*, *5*, 5452. https://doi.org/10.1038/ncomms6452

Birk, U. J. (2019). Super-resolution microscopy of chromatin. *Genes*, *10*(7). 493. https://doi.org/10.3390/genes10070493

Blinzinger, K., & Kreutzberg, G. (1968). Displacement of synaptic terminals from regenerating motoneurons by microglial cells. *Zeitschrift Für Zellforschung Und Mikroskopische Anatomie*, *85*(2), 145–157. https://doi.org/10.1007/BF00325030

Bolte, S., & Cordelières, F. P. (2006). A guided tour into subcellular colocalization analysis in light microscopy. *Journal of Microscopy*, *224*(Pt 3), 213–232. https://doi.org/10.1111/j.1365-2818.2006.01706.x

Bretschneider, S., Eggeling, C., & Hell, S. W. (2007). Breaking the diffraction barrier in fluorescence microscopy by optical shelving. *Physical Review Letters*, *98*(21), 218103. https://doi.org/10.1103/PhysRevLett.98.218103

Chen, S. K., Tvrdik, P., Peden, E., Cho, S., Wu, S., Spangrude, G., & Capecchi, M. R.. (2010). Hematopoietic origin of pathological grooming in Hoxb8 mutant mice. *Cell*, *141*(5), 775–785. https://doi.org/10.1016/j.cell.2010.03.055

Cizeron, M., Qiu, Z., Koniaris, B., Gokhale, R., Komiyama, N. H., Fransén, E., & Grant, S. G.. (2020). A brainwide atlas of synapses across the mouse life span. *Science*, *369*(6501), 270–275.

Coltharp, C., & Xiao, J. (2012). Superresolution microscopy for microbiology. *Cellular Microbiology*, *14*(12), 1808–1818. https://doi.org/10.1111/cmi.12024

Damisah, E. C., Hill, R. A., Rai, A., Chen, F., Rothlin, C. V., Ghosh, S., & Grutzendler, J.. (2020). Astrocytes and microglia play orchestrated roles and respect phagocytic territories during neuronal corpse removal *in vivo*. Science. *Advances*, *6*(26), eaba3239. https://doi.org/10.1126/sciadv.aba3239

Dani, A., Huang, B., Bergan, J., Dulac, C., & Zhuang, X. (2010). Superresolution imaging of chemical synapses in the brain. *Neuron*, *68*(5), 843–856. https://doi.org/10.1016/j.neuron.2010.11.021

Dickson, R. M., Cubitt, A. B., Tsien, R. Y., & Moerner, W. E. (1997). On/off blinking and switching behaviour of single molecules of green fluorescent protein. *Nature*, *388*(6640), 355–358. https://doi.org/10.1038/41048

Eugenín, E. A., Eckardt, D., Theis, M., Willecke, K., Bennett, M. V., & Saez, J. C. (2001). Microglia at brain stab wounds express connexin 43 and *in vitro* form functional gap junctions after treatment with interferon-gamma and tumor necrosis factor-alpha. *Proceedings of the National Academy of Sciences of the United States of America*, *98*(7), 4190–4195.

Fang, K., Chen, X., Li, X., Shen, Y., Sun, J., Czajkowsky, D. M., & Shao, Z.. (2018). Super-resolution imaging of individual human subchromosomal regions *in situ* reveals nanoscopic building blocks of higher-order structure. *ACS Nano*, *12*(5), 4909–4918.

Fernandez-Suarez, M., & Ting, A. Y. (2008). Fluorescent probes for super-resolution imaging in living cells. *Nature Reviews Molecular Cell Biology*, *9*(12), 929–943. https://doi.org/10.1038/nrm2531

Fölling, J., Bossi, M., Bock, H., Medda, R., Wurm, C. A., Hein, B., Jakobs, S., Eggeling, C., & Hell, S. W.. (2008). Fluorescence nanoscopy by ground-state depletion and single-molecule return. *Nature Methods*, *5*(11), 943–945. https://doi.org/10.1038/nmeth.1257

Galbraith, C. G., & Galbraith, J. A. (2011). Super-resolution microscopy at a glance. *Journal of Cell Science*, *124*(Pt 10), 1607–1611. https://doi.org/10.1242/jcs.080085

Garcia, A., Huang, D., Righolt, A., Righolt, C., Kalaw, M. C., Mathur, S., McAvoy, E., Anderson, J., Luedke, A., Itorralba, J., & Mai, S.. (2017). Super-resolution structure of DNA significantly differs in buccal cells of controls and Alzheimer's patients. *Journal of Cellular Physiology*, *232*(9), 2387–2395. https://doi.org/10.1002/jcp.25751

Ginhoux, F., Lim, S., Hoeffel, G., Low, D., & Huber, T. (2013). Origin and differentiation of microglia. *Frontiers in Cellular Neuroscience*, *7*, 45. https://doi.org/10.3389/fncel.2013.00045

Giulian, D., Haverkamp, L. J., Yu, J. H., Karshin, W., Tom, D., Li, J., Kirkpatrick, J., Kuo, Y. M., & Roher, A. E.. (1996). Specific domains of beta-amyloid from Alzheimer plaque elicit neuron killing in human microglia. *Journal of Neuroscience*, *16*(19), 6021–6037.

Gomez-Isla, T., Hollister, R., West, H., Mui, S., Growdon, J. H., Petersen, R. C., Parisi, J. E., & Hyman, B. T.. (1997). Neuronal loss correlates with but exceeds neurofibrillary tangles in Alzheimer's disease. *Annals of Neurology*, *41*(1), 17–24. https://doi.org/10.1002/ana.410410106

Graeber, M. B. (2010). Changing face of microglia. *Science*, *330*(6005), 783–788. https://doi.org/10.1126/science.1190929

Graeber, M. B. (2014). Neuroinflammation: No rose by any other name. *Brain Pathology*, *24*(6), 620–622. https://doi.org/10.1111/bpa.12192

Graeber, M. B., Bise, K., & Mehraein, P. (1993). Synaptic stripping in the human facial nucleus. *Acta Neuropathologica.*, *86*(2), 179–181. https://doi.org/10.1007/BF00334886

Graeber, M. B., & Kreutzberg, G. W. (1988). Delayed astrocyte reaction following facial nerve axotomy. *Journal of Neurocytology*, *17*(2), 209–220. https://doi.org/10.1007/BF01674208

Graeber, M. B., Streit, W. J., & Kreutzberg, G. W. (1988). Axotomy of the rat facial nerve leads to increased CR3 complement receptor expression by activated microglial cells. *Journal of Neuroscience Research*, *21*(1), 18–24. https://doi.org/10.1002/jnr.490210104

Hell, S. W. (2007). Far-field optical nanoscopy. *Science*, *316*(5828), 1153–1158. https://doi.org/10.1126/science.1137395

Helmuth, J. A., Paul, G., & Sbalzarini, I. F. (2010). Beyond co-localization: Inferring spatial interactions between sub-cellular structures from microscopy images. *BMC Bioinformatics*, *11*, 372. https://doi.org/10.1186/1471-2105-11-372

Hong, S., Beja-Glasser, V. F., Nfonoyim, B. M., Frouin, A., Li, S., Ramakrishnan, S., Merry, K. M., Shi, Q., Rosenthal, A., Barres, B. A., Lemere, C. A., Selkoe, D. J., & Stevens, B.. (2016). Complement and microglia mediate early synapse loss in Alzheimer mouse models. *Science*, *352*(6286), 712–716. https://doi.org/10.1126/science.aad8373

Hyman, B. T., Phelps, C. H., Beach, T. G., Bigio, E. H., Cairns, N. J., Carrillo, M. C., Dickson, D. W., Duyckaerts, C., Frosch, M. P., Masliah, E., Mirra, S. S., Nelson, P. T., Schneider, J. A., Thal, D. R., Thies, B., Trojanowski, J. Q., Vinters, H. V., & Montine, T. J.. (2012). National Institute on Aging-Alzheimer's Association guidelines for the neuropathologic assessment of Alzheimer's disease. *Alzheimer's & Dementia: the Journal of the Alzheimer's Association*, *8*(1), 1–13. https://doi.org/10.1016/j.jalz.2011.10.007

Ji, K., Akgul, G., Wollmuth, L. P., & Tsirka, S. E. (2013). Microglia actively regulate the number of functional synapses. *PLoS One*, *8*(2), e56293. https://doi.org/10.1371/journal.pone.0056293

Kreutzberg, G. W. (1996). Microglia: A sensor for pathological events in the CNS. *Trends in Neurosciences*, *19*(8), 312–318. https://doi.org/10.1016/0166-2236(96)10049-7

Lalkens, B., Testa, I., Willig, K. I., & Hell, S. W. (2012). MRT letter: Nanoscopy of protein colocalization in living cells by STED and GSDIM. *Microscopy Research and Technique*, *75*(1), 1–6. https://doi.org/10.1002/jemt.21026

Lim, S. H., Park, E., You, B., Jung, Y., Park, A. R., Park, S. G., & Lee, J.-R.. (2013). Neuronal synapse formation induced by microglia and

interleukin 10. *PLoS One*, *8*(11), e81218. https://doi.org/10.1371/journal.pone.0081218

Liu, X. B., & Schumann, C. M. (2014). Optimization of electron microscopy for human brains with long-term fixation and fixed-frozen sections. *Acta Neuropathologica Communications*, *2*, 42. https://doi.org/10.1186/2051-5960-2-42

Miyamoto, A., Wake, H., Moorhouse, A. J., & Nabekura, J. (2013). Microglia and synapse interactions: Fine tuning neural circuits and candidate molecules. *Frontiers in Cellular Neuroscience*, *7*, 70. https://doi.org/10.3389/fncel.2013.00070

Mockl, L., Lamb, D. C., & Brauchle, C. (2014). Super-resolved fluorescence microscopy: Nobel Prize in Chemistry 2014 for Eric Betzig, Stefan Hell, and William E. Moerner. *Angewandte Chemie International Edition*, *53*(51), 13972–13977.

Moerner, W. E. (2012). Microscopy beyond the diffraction limit using actively controlled single molecules. *Journal of Microscopy*, *246*(3), 213–220. https://doi.org/10.1111/j.1365-2818.2012.03600.x

Montine, T. J., Phelps, C. H., Beach, T. G., Bigio, E. H., Cairns, N. J., Dickson, D. W., Duyckaerts, C., Frosch, M. P., Masliah, E., Mirra, S. S., Nelson, P. T., Schneider, J. A., Thal, D. R., Trojanowski, J. Q., Vinters, H. V., & Hyman, B. T. (2012). National Institute on Aging-Alzheimer's Association guidelines for the neuropathologic assessment of Alzheimer's disease: A practical approach. *Acta Neuropathologica*, *123*(1), 1–11. https://doi.org/10.1007/s00401-011-0910-3

Moran, L. B., & Graeber, M. B. (2004). The facial nerve axotomy model. *Brain Research. Brain Research Reviews*, *44*(2–3), 154–178. https://doi.org/10.1016/j.brainresrev.2003.11.004

Nimmerjahn, A., Kirchhoff, F., & Helmchen, F. (2005). Resting microglial cells are highly dynamic surveillants of brain parenchyma *in vivo*. *Science*, *308*(5726), 1314–1318. https://doi.org/10.1126/science.1110647

Paasila, P. J., Davies, D. S., Goldsbury, C., & Sutherland, G. T. (2020). Clustering of activated microglia occurs before the formation of dystrophic neurites in the evolution of Aβ plaques in Alzheimer's disease. *Free Neuropathology*, *1*(20). https://doi.org/10.17879/freeneuropathology-2020-2845

Paasila, P. J., Davies, D. S., Kril, J. J., Goldsbury, C., & Sutherland, G. T. (2019). The relationship between the morphological subtypes of microglia and Alzheimer's disease neuropathology. *Brain Pathology*, *29*(6), 726–740. https://doi.org/10.1111/bpa.12717

Paolicelli, R. C., Bolasco, G., Pagani, F., Maggi, L., Scianni, M., Panzanelli, P., Giustetto, M., Ferreira, T. A., Guiducci, E., Dumas, L., Ragozzino, D., & Gross, C. T.. (2011). Synaptic pruning by microglia is necessary for normal brain development. *Science*, *333*(6048), 1456–1458. https://doi.org/10.1126/science.1202529

Paparelli, L., Corthout, N., Pavie, B., Wakefield, D. L., Sannerud, R., Jovanovic-Talisman, T., Annaert, W., & Munck, S. (2016). Inhomogeneity based characterization of distribution patterns on the plasma membrane. *PLoS Computational Biology*, *12*(9), e1005095. https://doi.org/10.1371/journal.pcbi.1005095

Parkhurst, C. N., Yang, G., Ninan, I., Savas, J. N., Yates, J. R., 3rd, Lafaille, J. J., Hempstead, B. L., Littman, D. R., & Gan, W.-B.. (2013). Microglia promote learning-dependent synapse formation through brain-derived neurotrophic factor. *Cell*, *155*(7), 1596–1609. https://doi.org/10.1016/j.cell.2013.11.030

Rankin, B. R., Moneron, G., Wurm, C. A., Nelson, J. C., Walter, A., Schwarzer, D., Schroeder, J., Colón-Ramos, D. A., & Hell, S. W.. (2011). Nanoscopy in a living multicellular organism expressing GFP. *Biophysical Journal*, *100*(12), L63–L65. https://doi.org/10.1016/j.bpj.2011.05.020

Ries, J., Kaplan, C., Platonova, E., Eghlidi, H., & Ewers, H. (2012). A simple, versatile method for GFP-based super-resolution microscopy via nanobodies. *Nature Methods*, *9*(6), 582–584. https://doi.org/10.1038/nmeth.1991

Sajjan, S., Holsinger, R. M., Fok, S., Ebrahimkhani, S., Rollo, J. L., Banati, R. B., & Graeber, M.. (2014). Up-regulation of matrix metallopeptidase 12 in motor neurons undergoing synaptic stripping. *Neuroscience*, *274*, 331–340. https://doi.org/10.1016/j.neuroscience.2014.05.052

Sarmiento, M. (2013). Use of confocal microscopy in the study of microglia in a brain metastasis model. *Methods in Molecular Biology*, *1041*, 337–346.

Schafer, D. P., Lehrman, E. K., Kautzman, A. G., Koyama, R., Mardinly, A. R., Yamasaki, R., Ransohoff, R. M., Greenberg, M. E., Barres, B. A., & Stevens, B.. (2012). Microglia sculpt postnatal neural circuits in an activity and complement-dependent manner. *Neuron*, *74*(4), 691–705. https://doi.org/10.1016/j.neuron.2012.03.026

Schafer, D. P., Lehrman, E. K., & Stevens, B. (2013). The, "quad-partite" synapse: Microglia-synapse interactions in the developing and mature CNS. *Glia*, *61*(1), 24–36. https://doi.org/10.1002/glia.22389

Schermelleh, L., Ferrand, A., Huser, T., Eggeling, C., Sauer, M., Biehlmaier, O., & Drummen, G. P.. (2019). Super-resolution microscopy demystified. *Nature Cell Biology*, *21*(1), 72–84. https://doi.org/10.1038/s41556-018-0251-8

Schermelleh, L., Heintzmann, R., & Leonhardt, H. (2010). A guide to super-resolution fluorescence microscopy. *Journal of Cell Biology*, *190*(2), 165–175. https://doi.org/10.1083/jcb.201002018

Shivanandan, A., Radenovic, A., & Sbalzarini, I. F. (2013). MosaicIA: An ImageJ/Fiji plugin for spatial pattern and interaction analysis. *BMC Bioinformatics*, *14*, 349. https://doi.org/10.1186/1471-2105-14-349

Sieben, C., Douglass, K. M., Guichard, P., & Manley, S. (2018). Super-resolution microscopy to decipher multi-molecular assemblies. *Current Opinion in Structural Biology*, *49*, 169–176. https://doi.org/10.1016/j.sbi.2018.03.017

Sigrist, S. J., & Sabatini, B. L. (2012). Optical super-resolution microscopy in neurobiology. *Current Opinion in Neurobiology*, *22*(1), 86–93. https://doi.org/10.1016/j.conb.2011.10.014

Sreedharan, S., Gill, M. R., Garcia, E., Saeed, H. K., Robinson, D., Byrne, A., Cadby, A., Keyes, T. E., Smythe, C., Pellett, P., Bernardino de la Serna, J., & Thomas, A.. (2017). Multimodal super-resolution optical microscopy using a transition-metal-based probe provides unprecedented capabilities for imaging both nuclear chromatin and mitochondria. *Journal of the American Chemical Society*, *139*(44), 15907–15913. https://doi.org/10.1021/jacs.7b08772

Stracy, M., & Kapanidis, A. N. (2017). Single-molecule and super-resolution imaging of transcription in living bacteria. *Methods*, *120*, 103–114. https://doi.org/10.1016/j.ymeth.2017.04.001

Streit, W. J., Braak, H., Xue, Q. S., & Bechmann, I. (2009). Dystrophic (senescent) rather than activated microglial cells are associated with tau pathology and likely precede neurodegeneration in Alzheimer's disease. *Acta Neuropathologica*, *118*(4), 475–485. https://doi.org/10.1007/s00401-009-0556-6

Sutherland, G. T., Sheedy, D., Stevens, J., McCrossin, T., Smith, C. C., van Roijen, M., & Kril, J. J.. (2016). The NSW brain tissue resource centre: Banking for alcohol and major neuropsychiatric disorders research. *Alcohol*, *52*, 33–39. https://doi.org/10.1016/j.alcohol.2016.02.005

Svahn, A. J., Becker, T. S., & Graeber, M. B. (2014). Emergent properties of microglia. *Brain Pathology*, *24*(6), 665–670. https://doi.org/10.1111/bpa.12195

Svahn, A. J., Graeber, M. B., Ellett, F., Lieschke, G. J., Rinkwitz, S., Bennett, M. R., & Becker, T. S.. (2013). Development of ramified microglia from early macrophages in the zebrafish optic tectum. *Developmental Neurobiology*, *73*(1), 60–71. https://doi.org/10.1002/dneu.22039

Terry, R. D., Masliah, E., Salmon, D. P., Butters, N., DeTeresa, R., Hill, R., Hansen, L. A., & Katzman, R.. (1991). Physical basis of cognitive alterations in Alzheimer's disease: Synapse loss is the major correlate of cognitive impairment. *Annals of Neurology*, *30*(4), 572–580. https://doi.org/10.1002/ana.410300410

Thompson, M. A., Lew, M. D., & Moerner, W. E. (2012). Extending microscopic resolution with single-molecule imaging and active control.

Annual Review of Biophysics, *41*, 321–342. https://doi.org/10.1146/annurev-biophys-050511-102250

Tischer, J., Krueger, M., Mueller, W., Staszewski, O., Prinz, M., Streit, W. J., & Bechmann, I.. (2016). Inhomogeneous distribution of Iba-1 characterizes microglial pathology in Alzheimer's disease. *Glia*, *64*(9), 1562–1572. https://doi.org/10.1002/glia.23024

Tremblay, M., Lowery, R. L., & Majewska, A. K. (2010). Microglial interactions with synapses are modulated by visual experience. *PLoS Biology*, *8*(11), e1000527. https://doi.org/10.1371/journal.pbio.1000527

Tzioras, M., Daniels, M. J. D., King, D., Popovic, K., Holloway, R. K., Stevenson, A. J., Tulloch, J., Kandasamy, J., Sokol, D., Latta, C., Rose, J., Smith, C., Miron, V. E., Henstridge, C., McColl, B. W., & Spires-Jones, T. L.. (2019). Altered synaptic ingestion by human microglia in Alzheimer's disease. *bioRxiv*. https://doi.org/10.1101/795930

van de Linde, S. (2019). Single-molecule localization microscopy analysis with ImageJ. *Journal of Physics. D. Applied Physics*, *52*(20), 203002. https://doi.org/10.1088/1361-6463/ab092f

Vasek, M. J., Garber, C., Dorsey, D., Durrant, D. M., Bollman, B., Soung, A., Yu, J., Perez-Torres, C., Frouin, A., Wilton, D. K., Funk, K., DeMasters, B. K., Jiang, X., Bowen, J. R., Mennerick, S., Robinson, J. K., Garbow, J. R., Tyler, K. L., Suthar, M. S., … Klein, R. S.. (2016). A complement-microglial axis drives synapse loss during virus-induced memory impairment. *Nature*, *534*(7608), 538–543. https://doi.org/10.1038/nature18283

Vaziri, A., Tang, J., Shroff, H., & Shank, C. V. (2008). Multilayer three-dimensional super resolution imaging of thick biological samples. *Proceedings of the National Academy of Sciences of the United States of America*, *105*(51), 20221–20226. https://doi.org/10.1073/pnas.0810636105

Wake, H., Moorhouse, A. J., Jinno, S., Kohsaka, S., & Nabekura, J. (2009). Resting microglia directly monitor the functional state of synapses *in vivo* and determine the fate of ischemic terminals. *Journal of Neuroscience*, *29*(13), 3974–3980. https://doi.org/10.1523/JNEUROSCI.4363-08.2009

Wang, C., Yue, H., Hu, Z., Shen, Y., Ma, J., Li, J., Wang, X.-D., Wang, L., Sun, B., Shi, P., Wang, L., & Gu, Y.. (2020). Microglia mediate forgetting via complement-dependent synaptic elimination. *Science*, *367*(6478), 688–694. https://doi.org/10.1126/science.aaz2288

Wasseff, S. K., & Scherer, S. S. (2014). Activated microglia do not form functional gap junctions *in vivo*. *Journal of Neuroimmunology*, *269*(1–2), 90–93. https://doi.org/10.1016/j.jneuroim.2014.02.005

Watanabe, S., Lehmann, M., Hujber, E., Fetter, R. D., Richards, J., Söhl-Kielczynski, B., Felies, A., Rosenmund, C., Schmoranzer, J., & Jorgensen, E. M.. (2014). Nanometer-resolution fluorescence electron microscopy (nano-EM) in cultured cells. *Methods in Molecular Biology*, *1117*, 503–526.

Weinhard, L., di Bartolomei, G., Bolasco, G., Machado, P., Schieber, N. L., Neniskyte, U., Exiga, M., Vadisiute, A., Raggioli, A., Schertel, A., Schwab, Y., & Gross, C. T.. (2018). Microglia remodel synapses by presynaptic trogocytosis and spine head filopodia induction. *Nature Communications*, *9*(1), 1228. https://doi.org/10.1038/s41467-018-03566-5

Westerfield, M. (2000). *The zebrafish book: A guide for the laboratory use of zebrafish* (Danio rerio). University of Oregon.

Wu, Y., Dissing-Olesen, L., MacVicar, B. A., & Stevens, B. (2015). Microglia: Dynamic mediators of synapse development and plasticity. *Trends in Immunology*, *36*(10), 605–613. https://doi.org/10.1016/j.it.2015.08.008

Xu, J., & Liu, Y. (2019). A guide to visualizing the spatial epigenome with super-resolution microscopy. *FEBS Journal*, *286*(16), 3095–3109. https://doi.org/10.1111/febs.14938

Yamamoto, S., Nakajima, K., & Kohsaka, S. (2010). Macrophage-colony stimulating factor as an inducer of microglial proliferation in axotomized rat facial nucleus. *Journal of Neurochemistry*, *115*(4), 1057–1067. https://doi.org/10.1111/j.1471-4159.2010.06996.x

Zhan, Y., Paolicelli, R. C., Sforazzini, F., Weinhard, L., Bolasco, G., Pagani, F., Vyssotski, A. L., Bifone, A., Gozzi, A., Ragozzino, D., & Gross, C. T.. (2014). Deficient neuron-microglia signaling results in impaired functional brain connectivity and social behavior. *Nature Neuroscience*, *17*(3), 400–406. https://doi.org/10.1038/nn.3641

SUPPORTING INFORMATION

Additional supporting information may be found online in the Supporting Information section.

Supplementary Material

Transparent Science Questionnaire for Authors

Transparent Peer Review Report

How to cite this article: Paasila PJ, Fok SYY, Flores-Rodriguez N, et al. Ground state depletion microscopy as a tool for studying microglia–synapse interactions. *J Neurosci Res*. 2021;99:1515–1532. https://doi.org/10.1002/jnr.24819